Overcoming sensor constraints in 3D integral imaging

Manuel Martínez-Corral*, Raúl Martínez-Cuenca, Genaro Saavedra, Bahram Javidi+
Department of Optics, University of Valencia, E46100 Burjassot, Spain
+Electrical and Computer Engineering Dept, University of Connecticut, Storrs, CT 06269-1157

ABSTRACT

One of the main challenges in integral imaging is to overcome the limited depth of field. Although it is widely assumed that such limitation is mainly imposed by diffraction due to lenslet imaging, we show that the most restricting factor is the pixelated structure of the sensor (CCD). In this context, we take profit from these sensor constraints and demonstrate that by proper binary amplitude modulation of the pickup microlenses, the depth of field can be substantially improved with no deterioration of lateral resolution.

Key words: Three-dimensional image acquisition, Multiple imaging, Resolution, Depth of field.

1. INTRODUCTION

Currently, much visual information is presented to users through computer monitors, TV screens, or even through cellular-phone or PDA screens. The displayed images can have entertainment or information values, or even be aimed at the diffusion of research results [1]. The information society increasingly demands the display of not only plane images but also of three-dimensional (3D) images, or even movies [2-5], with continuous perspective information. Although the search for optimum 3D imaging and display techniques has been the subject of research from much more than for a century [6], it has been in the last several years when technology is approaching the level required for realization of 3D imaging systems. The so-called integral imaging (InI), which is a 3D imaging technique specially suited for the above requirements, works with incoherent light, and provides with auto-stereoscopic images without the help of any special glasses. In an InI system, an array of microlenses generates, onto a sensor such as a CCD, a collection of plane elemental images. Each elemental image has a different perspective of the 3D object. Therefore, the CCD records the projections of the object. In the reconstruction stage, the recorded images are displayed by an optical device, such as a LCD monitor, placed in front of another microlens array. This setup provides the observer with a reconstructed 3D image with full paralax. Integral imaging was first proposed by Lippmann [7], and some relevant work was done in the meantime [8-12]. The interest in InI has been resurrected recently because of its application to 3D TV and display [13].

Since its rebirth, InI has overcome many of its challenges. Specifically, it is remarkable that a simple technique for the pseudoscopic to orthoscopic conversion was developed [14]. Some methods were proposed to overcome the limits in lateral resolution imposed by the CCD [15-17], or by the microlens array [18,19]. Other challenge satisfactorily faced is of the limitation in viewing area [22]. Apart from this engineering work, some purely theoretical work has been also performed to characterize the response in resolution of InI systems [23,24], or the viewing parameters in the display stage [25,26].

At present 3D InI systems still face some problems. One issue is the limited depth of field (DOF). In a typical scene objects exist at different depth positions. Since only a single plane is used to capture the images, it is not possible for all objects to be in focus. Then blurred images of out-of-focus objects, or part of objects, are obtained. Although the DOF of integral imaging systems is influenced by many parameters (related with both the capture and the display systems), it is apparent that to display a clear integral image of an axially elongated 3D object it is essential to capture sharp 2D elemental images of it. For this reason, the bottleneck of the DOF in integral imaging is the limited depth of focus of the microlens array used in the pickup stage. One could overcome this problem by reducing the numerical aperture (NA) of the lenses. However, such a reduction would produce, as a collateral effect, a worsening of lateral resolution of capture stage, and therefore of spatial resolution of the overall integral imaging system. In the past few years, some new alternative techniques have been proposed to improve the depth of field of integral imaging systems. These methods are based on the synthesis of real and virtual image fields [27], or on the use of lenses with non-uniform focal lengths and aperture sizes [28,29].

* manuel.martinez@uv.es; phone +34 96354 4718; fax +34 96354 4715; www.uv.es/imaging3

Unmanned/Unattended Sensors and Sensors Networks II,
Edited by Edward M. Carapezza, Proc. of SPIE Vol. 5986
598604, (2005) · doi: 10.1117/12.633488

In this paper we propose a new method for producing a significant enlargement of the depth of field of the integral-imaging pickup system. This enlargement is not accompanied by a deterioration of spatial resolution. The method, whose main feature is its simplicity, is based on an adequate binary modulation of the microlenses amplitude transmittance [30]. To present our technique we start by carrying out a theoretical analysis of the pickup stage of integral imaging systems, in terms of the scalar diffraction theory. This analysis explicitly takes into account the fact that the object is a surface object. This assumption allows us to develop a set of equations, which constitutes a strict description of the diffractive behavior of the pickup of an integral imaging system. This analysis shows us that, conversely to what is generally assumed, integral imaging systems are not linear and shift invariant, and therefore it is not valid, *stricto senso*, to define neither a point spread function (PSF) nor an optical transfer function (OTF). In a second step, we design an adequate amplitude modulator, which should be applied to any element of the microlens array. Later, we explain how to overcome the sensor constraints. In fact we take advantages of them to propose a technique for important enlargement of the DOF [31]. We have performed numerical simulations with computer-synthesized objects, to show that the DOF of focus is significantly improved.

2. THEORETICAL ANALYSIS OF THE CAPTURE STAGE

To discuss the method we start by describing the capture stage from the point of view of diffraction theory. Let us remark that since the microlens arrays generally used in typical InI experiments are of low numerical aperture ($NA \approx 0.1$), the analysis can be accurately performed within the frame of the paraxial scalar diffraction theory. In Fig. 1 we show a scheme of the capture setup. Spatial coordinates are denoted $\mathbf{x} = (x, y)$ and z for directions transverse and parallel to the system main optical axis. We consider a surface object under spatially incoherent illumination. For simplicity we assume quasi-monochromatic illumination with mean wavelength λ. Light emitted by the surface object is collected by the microlens array to form a collection of 2D elemental aerial images. The images are formed in the so-called aerial pickup plane, which is set at a distance g from the microlens array. The reference and the aerial pickup plane are conjugated through the microlenses, so that distances a and g are related by the lens law $1/a+1/g-1/f=0$. Any elemental image has a different perspective of the surface object. In our scheme a relay system, composed by a field lens and a camera lens, is used to image the aerial images into the pickup device (usually a CCD camera). The lateral magnification of the relay system is adjusted so that the size of the elemental-images collection array matches the CCD.

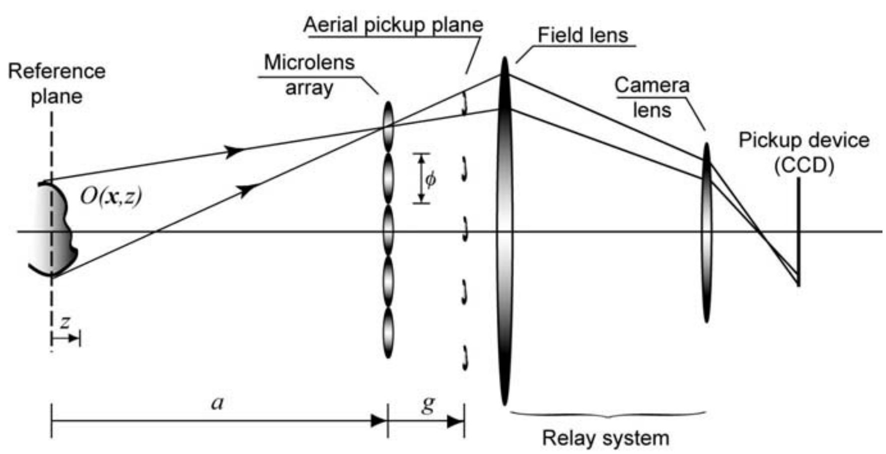

Figure 1. Scheme, not to scale, of the capture setup of a 3D InI system. Object points out of reference plane produce blurred images in the CCD. In the relay system the field lens collects the rays from the outer microlenses; the camera lens projects the images onto the CCD.

The intensity distribution of incoherent light scattered by the object can be represented by the real and positive function

$$O(\mathbf{x}, z) = R(\mathbf{x})\delta(z - f(\mathbf{x})) \ , \qquad (1)$$

where function $R(\mathbf{x})$ accounts for the object intensity reflectivity, whereas $f(\mathbf{x}) - z = 0$ is the function that describes the surface.

We consider now the light scattered at an arbitrary point $(\mathbf{x}, z)$ of the surface object. It is straightforward, by application in cascade of paraxial scalar diffraction equations, to find that the intensity at a given point $\mathbf{x'} = (x', y')$ of the aerial pickup plane is given by

$$H_\lambda(\mathbf{x'}; \mathbf{x}, z) = \left| \sum_{\mathbf{m}} \exp\left\{ i \frac{\pi}{\lambda(a-z)} |\mathbf{m}p - \mathbf{x}|^2 \right\} \int \mathsf{P}_z(\mathbf{x_o}) \exp\left\{ -i2\pi \mathbf{x_o} \frac{\mathbf{x'} + [M_z(\mathbf{m}p - \mathbf{x}) - \mathbf{m}p]}{\lambda g} \right\} d^2\mathbf{x_o} \right|^2, \tag{2}$$

where $\mathbf{m}=(m,n)$ accounts for the microlenses indexes in the (x,y) directions, and p stands for the constant pitch of the microlens array. In Eq. (2) $M_z=-g/(a-z)$ is a magnification factor that depends on the depth coordinate z. The so-called generalized pupil function is:

$$\mathsf{P}_z(\mathbf{x_o}) = p(\mathbf{x_o}) \exp\left\{ i \frac{\pi}{\lambda} \left(\frac{1}{a-z} - \frac{1}{a} \right) |\mathbf{x_o}|^2 \right\}. \tag{3}$$

This function accounts for the microlenses pupil function, $p(\mathbf{x_o})$, together with the phase modulation due to defocus errors. It is important to remark that, in principle, the matter of interest of our research is not the intensity distribution at the aerial pickup plane, but the distribution at the pickup-device plane. Note however that since such a distribution is simply a uniformly scaled version of the one in Eq. (2), it is correct to base our study on such an equation.

Assuming non significant overlapping between the elemental diffraction spots provided by the different microlenses, Eq. (2) can be rewritten in quite good approximation as the 2D convolution between the, properly scaled, 2D Fourier transform of $\mathsf{P}_z(\mathbf{x_o})$ and a sampling function, that is

$$H_\lambda(\mathbf{x'}; \mathbf{x}, z) = \left| \tilde{\mathsf{P}}_z\left(\frac{\mathbf{x'}}{\lambda g} \right) \right|^2 \otimes \sum_{\mathbf{m}} \delta\{\mathbf{x'} - [\mathbf{m}p(1 - M_z) + M_z \mathbf{x}]\}. \tag{4}$$

Let us consider now the overall light proceeding from the surface object. In this case the intensity distribution in the pickup plane is obtained as a weighted superposition of the diffraction spots provided by any point of the surface object, namely

$$I_\lambda(\mathbf{x'}) = \int R(\mathbf{x}) \delta(z - f(\mathbf{x})) H_\lambda(\mathbf{x'}; \mathbf{x}, z) d^2\mathbf{x}\, dz = \int R(\mathbf{x}) H_\lambda(\mathbf{x'}; \mathbf{x}, z = f(\mathbf{x})) d^2\mathbf{x} \tag{5}$$

Note that function $H_\lambda(\bullet)$ explicitly depends on $\mathbf{x'} - M_z \mathbf{x}$, that is:

$$H_\lambda(\mathbf{x'}; \mathbf{x}, z) = H_\lambda(\mathbf{x'} - M_z \mathbf{x}; 0, z) \equiv \mathcal{H}_\lambda(\mathbf{x'} - M_z \mathbf{x}; z). \tag{6}$$

Then, Eq. (5) can be rewritten as

$$I_\lambda(\mathbf{x'}) = \int R(\mathbf{x}) \mathcal{H}_\lambda(\mathbf{x'} - M_z \mathbf{x}; z = f(\mathbf{x})) d^2\mathbf{x}. \tag{7}$$

Although Eq. (7) seems to represent a 2D convolution, it does not. This is because function $\mathsf{P}_z(\mathbf{x_o})$ has a strong dependence on the axial position of the corresponding surface points. In other words, function $\mathcal{H}_\lambda(\bullet)$ is different for different values of z. Besides, factor M_z also depends on z, and therefore parts of the object at different depth are magnified in different way. Consequently, the impulse response is different at any depth. This fact implies that, the pickup system is not linear and shift invariant. Therefore, neither the PSF nor the OTF could be rigorously defined.

As seen above, the acquired image is composed by an array of elemental images of the surface object, each one obtained from a different viewpoint. Let us now focus our attention into the elemental image produced by one of the microlenses, for example the one in the center of the microlens array (this selection does not subtract any generality from our study). The intensity distribution of such an elemental image is given by

$$I_\lambda^{o}(\mathbf{x}') = \int R(\mathbf{x}) H_\lambda^{o}(\mathbf{x}' - M_z \mathbf{x}; z)\, d^2\mathbf{x} \quad , \tag{8}$$

where

$$H_\lambda^{o}(\mathbf{x}'; z) = \left| \tilde{P}_z\left(\frac{\mathbf{x}'}{\lambda g}\right)\right|^2 \quad . \tag{9}$$

We assume that the pupil of each microlens is a circle with diameter ϕ. In such a case, it is convenient to express Eq. (9) in cylindrical coordinates as follows

$$H_\lambda^{o}(r, z) = \left| \int_0^{\phi/2} p(r_o) \exp\left\{ i \frac{\pi}{\lambda} \frac{z}{a(a-z)} r_o^2 \right\} J_o\left(2\pi \frac{r\, r_o}{\lambda g}\right) r_o \; dr_o \right|^2 \quad . \tag{10}$$

3. THE BINARY AMPLITUDE MODULATION

In Fig. 2(a) we have represented some cross-sections of Eq. (10). The parameters for the calculation were: ϕ=2.0 mm, f=5.0 mm, λ=0.5 µm, and a=100 mm. Note that, due to the low value for the lens NA, the axial extent of H_λ^{o} is much higher than the lateral extent. In the section z=0 we can recognize the Airy disk pattern, whose extent determines the lateral resolution of the system. We find that in this case the resolution limit, as defined by Rayleigh, is of 1.61 µm, if measured in the pickup plane, or of 30.6 µm if evaluated in the reference object plane. The DOF is usually evaluated by means of the so-called Rayleigh range, which is defined as the extent of the axial interval in which $H_\lambda^{o}(0, z)$ is higher than $\sqrt{2}/2$ times its maximum value [32]. In this case, the Rayleigh range is $-3.3mm < z < 3.1mm$. Let us remark that, as we see in the following section, the pixel size of the capture device is a factor that strongly influences the DOF and the resolution. However, in our calculations at this stage we have considered that the pixels are sufficiently fine.

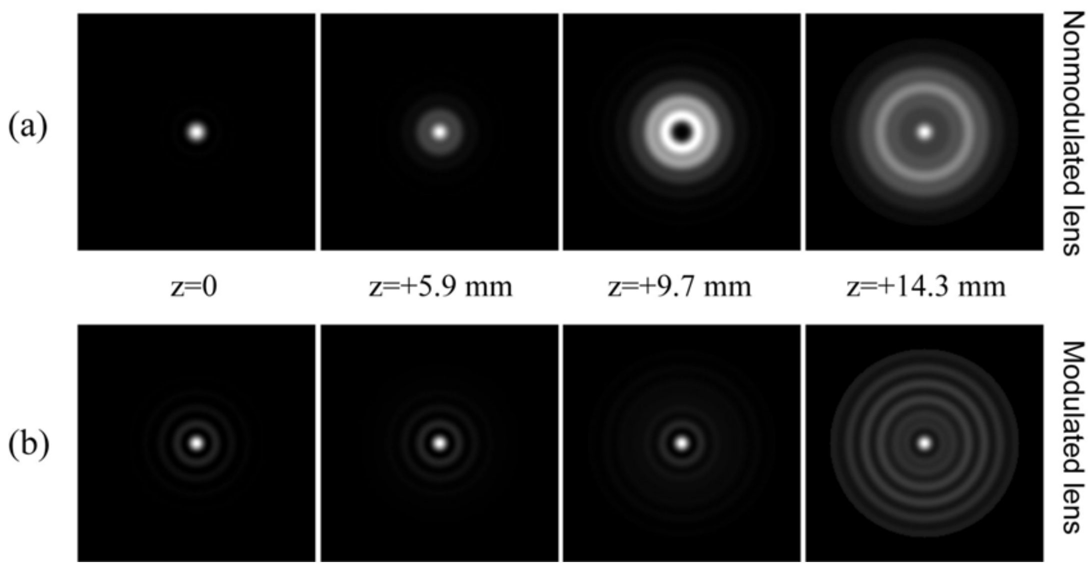

Figure 2. Cross sections of function $H_\lambda^{0}(\mathbf{x}, z)$ corresponding to: (a) the nonmodulated lenses; and (b) the amplitude-modulated lenses. The filters consist in an opaque circular mask of diameter $\delta\phi$ (with $\delta = 1/\sqrt{2}$) centered just behind each microlens.

To illustrate the limitations in DOF of an integral imaging system, we have performed a numerical experiment in which we obtain the elemental images of a computer-synthesized object. Since the aim of the experiment is to appreciate the improvement in DOF, we have selected as the object the Snellen **E** tumbling chart, which is usually used to grade resolution and defocus errors in visual optics. In the experiment the **E** patterns are positioned side by side and are longitudinally located at z_1=-10.0 *mm*, z_2=-5.0 *mm*, z_3=+4.6 *mm*, z_4=+8.3 *mm*, respectively, as depicted in Fig. 3. Note that the axial positions are not symmetric about the reference plane, but corresponds to the same amount of defocus as defined in terms of the well-known defocus coefficient $\omega_{20} = z\phi^2 / 2\lambda a(a-z)$ [33]. The elemental images were calculated according to Eq. (7). In Fig. 4(a) we show the central element **m**=(0,0). It is clear from the figure that the images of the **E** patterns in z_1 and z_4 are highly blurred. Let us remark that, since the imaging system is not telecentric [34], the images corresponding to planes with the same modulus of ω_{20} but different sign are different. This is due to the different scale of defocused images. Due to this effect, the elemental image of the **E** patterns located at z_1 is much more blurred than the elemental image corresponding to the **E** pattern at z_4. It is noticeable that in the case of the pattern at z_1 one can hardly distinguish the original orientation of the **E** in the elemental image.

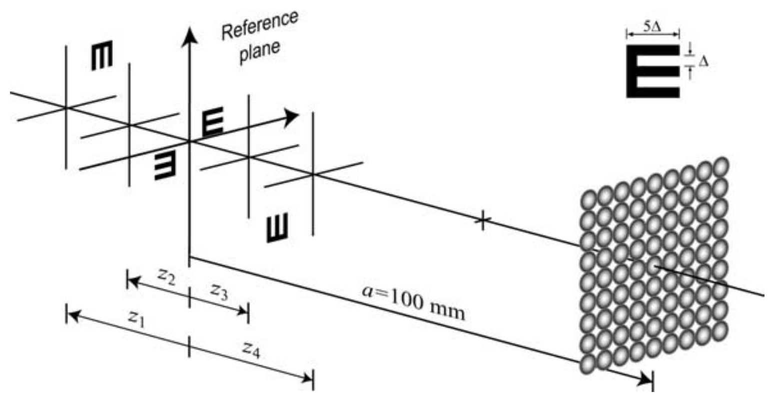

Figure 3. Scheme, not to scale, of the integral imaging numerical experiment. The size of the legs of the charts used in our experiments is $\Delta = 51\,\mu m$, which is about two times the Rayleigh resolution limit.

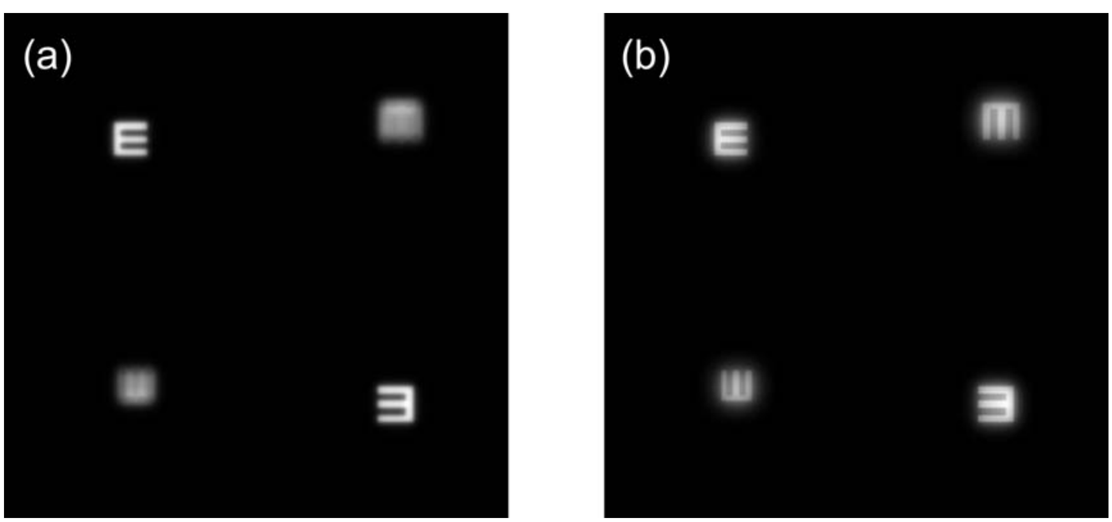

Figure 4. 2D central elemental images captured with the microlens array. We do not show the whole field of view, but only a portion of $0.4\,\text{mm} \times 0.4\,\text{mm}$ centered at the corresponding optical axis. (a) Image obtained with the non-modulated microlenses; (b) Image obtained with the amplitude-modulated microlenses.

The problem of the limited DOF can be overcome by use of amplitude-modulation techniques. Specifically we propose the use of binary amplitude modulators. Such kind of modulators have been successfully applied to improve the performance of other 3D imaging techniques such as confocal microscopy [35] or multiphoton scanning microscopy [36]. The technique consists in obscuring the central part of each microlens. Such an obscuration allows the secondary Huygens wavelets proceeding from the outer part of the lenses to interfere constructively in an enlarged axial range. Then by simply placing an opaque circular mask of diameter D=$\delta\phi$ (with $0<\delta<1$) just behind each microlens, one can increase the focal depth of the microlens array. It is known that the higher the value of the obscuration ratio δ, the broader the axial intensity spot. In an ideal case one could obtain infinite depth of focus by approaching the value of δ to the unity. However, such a situation is not convenient from an experimental point of view, because the higher the value of δ the smaller the light efficiency of the system. On the other hand, if one works with only the outermost part of the lenses, the optical aberrations of the system dramatically increase. For these reasons, we propose to use the binary modulator of obscuration ratio $\delta = \sqrt{2}/2$. This modulator has a light efficiency of 50%, and doubles the depth of focus of the system.

In Fig. 2(b), we have represented some cross-sections of Eq. (10), for the case of amplitude modulation with obscuration ratio $\delta = \sqrt{2}/2$. In this case, the Rayleigh resolution limit is 22.3 μm (as evaluated in the reference plane), whereas the DOF is -6.8 mm$<z<$+6.0 mm. If we compare these results with the ones obtained with the non-modulated setup (see Fig. 2(a)) we find that the DOF has been doubled, and the 2D density of resolved points has been increased by a factor of 1.85. Also in this case we have performed the numerical experiment with the same Snellen **E** tumbling chart as in the previous section. The central elemental image, $\mathbf{m}$=(0,0), is shown in Fig. 4(b). One observes the noticeable improvement in DOF provided by the amplitude modulation phase elements method. Note on the other hand, that the images of objects at z_2 and z_3 are slightly more blurred than the ones obtained with the non-modulated architecture. This fact seems to contradict the statement that the binary modulation improves the lateral resolution, as defined by Rayleigh, for objects placed at any depth z. Take into account, however, that the Rayleigh resolution limit is defined for point objects, and therefore it does not hold in case of more elaborated objects. In such a case, the use of binary amplitude modulation improves lateral resolution in a very large range of depth positions, but produces a slight worsening for low values of depth coordinate z.

4. THE INFLUENCE OF THE DETECTOR PIXEL SIZE

Let us revisit at this point the concepts of lateral resolution and DOF. The resolution of an imaging system evaluates its capacity for producing sharp images of the finest features of the object, when it is in focus. In case of diffraction-limited imaging systems, resolution is usually evaluated in terms of the Rayleigh criterion. According to it, the resolution of the pickup system under study is determined by the radius of the first zero ring of the Airy disk, $H_\lambda^{\mathbf{0}}(\mathbf{x},0)$. Note that the central lobe contains 84% of the energy in the Airy disk. On the other hand, The DOF of an imaging system is the distance by which the object may be axially shifted before an unacceptable blur is produced. In diffraction-limited imaging systems, the DOF is usually evaluated in terms of the so-called Rayleigh range: the axial distance from the in-focus plane to the point that produces an spot whose radius has increased by a factor $2^{1/2}$. The evaluation of the radii of the spots produced by out-of-focus points ($z\neq0$) is not as simple as in the in-focus case. This is because as z increases the spot spreads and neither a central lobe nor zero ring are recognized. In this case we define the defocused-spot diameter as the one of a circle that encircles 84% of the overall pattern energy. In mathematical terms such diameter, $D(z)$, is the one which solves the equation

$$\int_0^{D/2} H_\lambda^{0}(\mathbf{x},z)\,d\mathbf{x} = 0.84\int_0^{\infty} H_\lambda^{0}(\mathbf{x},z)\,d\mathbf{x}\ . \tag{11}$$

In Fig. 5(b) we represent, with thick line, the defocused-spot diameter for different values of distance z. We conclude, from the figure, that if only the limits imposed by diffraction are considered, the resolution limit of the pickup system under study is of is of 3.33 μm, measured in the aerial pickup plane, and the DOF is, for positive values of z, of +8.5 mm.

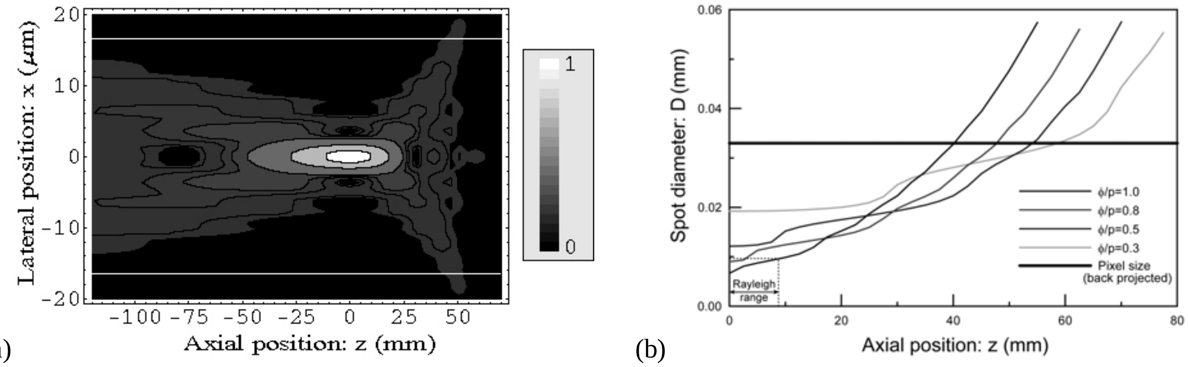

Figure 5. (a) Grey-scale representation of Eq. 10. Any cross-sections correspond to the spot produced by an object point at a depth z. White lines delimit the back-projected pixel size. The effect of defocus is much more appreciable for positive values of z; (b) Spot diameter for different values of the fill factor. The black thick line is used to mark the back-projected pixel size.

To appreciate the influence of pixelation on the lateral resolution at any depth position of the object, we assumed that the CCD has 1024x768 square pixels and the array has 34x25 microlenses. Therefore each elemental image has 30x30 pixels. In Fig. 5(a), we have drawn a pair of horizontal lines separated by a distance that equals the back projection of the pixel size onto the aerial pickup plane. When the intensity spot is smaller than the (back projected) pixel size, the resolution limit is imposed by the pixelated structure of the CCD. On the contrary, when the intensity spot is bigger than the pixel size, the resolution limit is imposed by diffraction. In Fig. 5(b) we have plotted a horizontal thick line that corresponds to the back-projected pixel size. From this figure, some important properties of the captured elemental images can be deduced: (a) The resolution limit for objects at z=0 is determined by the CCD pixel size. This limit is much higher than the one imposed by diffraction; (b) For objects in a large range of axial positions z, the resolution limit is still imposed by the CCD. Therefore this limit is the same as for objects at z=0; (c) For objects beyond the above range, the resolution is imposed by the spot diameter, which rapidly increases as z increases. (d) The range of axial positions in which the resolution limit does not change, defines now the DOF of the capture setup of an InI system.

Then we can conclude that, contrarily to what is commonly assumed, in a large rage of depth positions the lateral resolution of the capture setup is determined not by diffraction but by the CCD. This fact provides us with one additional degree of freedom in the design of the optimum pickup. Specifically, one can safely increase the DOF by use of techniques that in diffraction-limited systems would deteriorate the lateral resolution at z=0. In this sense, one can decrease the lenslets fill factor, defined as the quotient between the diameter of the microlenses, ϕ, and the pitch, p. It is known that decreasing the lenslets fill factor, produces the increase of the spot diameter at z=0, but a significant reduction for larger values of z. Reducing the fill factor does not affect to the lateral resolution at z=0 (which is determined by the CCD), but importantly increases the DOF. In Fig. 5(b), we have represented the evolution of the spot diameter for different values of the fill factor. All the cases represented have the same lateral resolution at low values for z. However,

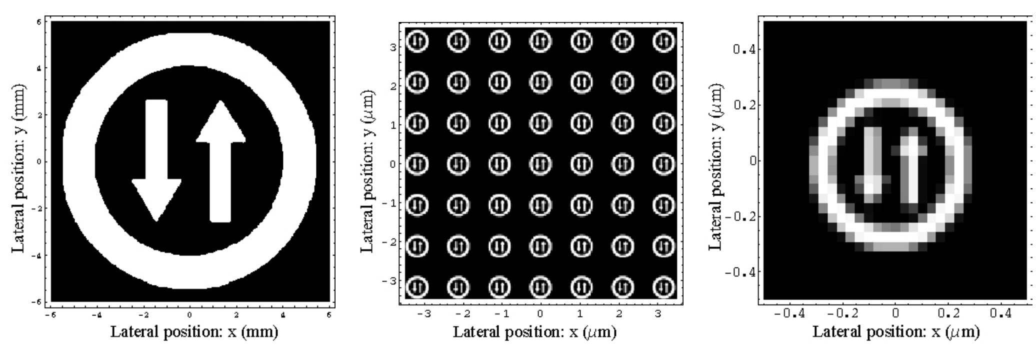

Figure 6. (a) Synthetic object; (b) 2D elemental images captured from 49 views; (c) Enlarged view of the central image. The object was placed at z=0 and the fill factor was set at ϕ/p=1.0

for example, the DOF obtained with ϕ/p=0.5 is 40% longer than the one obtained with ϕ/p=1.0. At z=54 mm the resolution limit obtained with ϕ/p=0.5 is half of the one obtained with a fill factor of 1.

To further illustrate our proposal, we have performed a numerical imaging experiment with a computer-generated synthetic object, see Fig 6(a). In the first step, we have calculated the elemental images assuming that the object was placed at z=0 and the fill factor is ϕ/p=1.0. The images captured from 49 different views are shown in Fig. 6(b). In Fig. 6(c) we show an enlarged image of the central element **m**=(0,0). Next, in Fig. 7, we show the elemental images obtained with the fill factor ϕ/p=0.5. There are no differences in resolution between this image and the one obtained with ϕ/p=1.0.

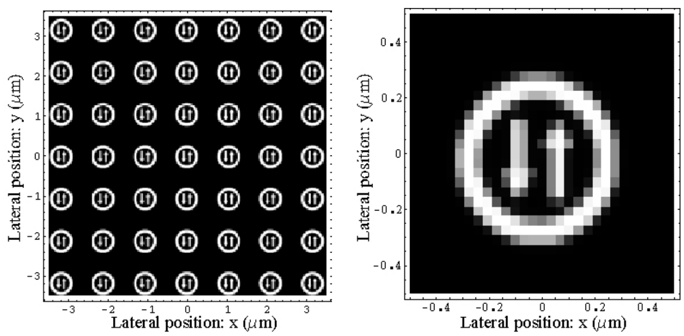

Figure 7. (a) 2D elemental images of the object captured from 49 different views; (b) Enlarged view of the central image. The object was placed at z=0 and the fill factor was set at ϕ/p=0.5.

In Fig. 8 we show the of the central elemental image obtained when the synthetic object is axially displaced to z=67.5 mm. Note that the magnification factor M_z increases with z. It is apparent that for large values of z the resolution obtained with ϕ/p=0.5 is much better than the resolution obtained with of ϕ/p=1.0.

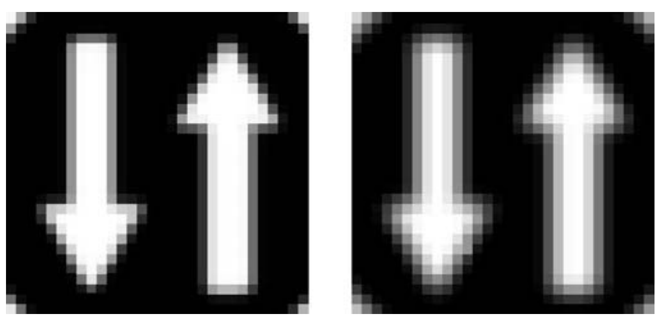

Figure 8. Central elemental image as the object is displaced from z=0 to z=67.5 mm. Left-hand image corresponds to ϕ/p=0.5. Right-hand one to ϕ/p=1.0.

5. CONCLUSIONS

We present a method for improvement of depth of field of 3D integral imaging with no deterioration of lateral resolution. The technique takes profit from the influence of pixelation on resolution of defocused objects. By proper binary amplitude modulation of the microlenses one can substantially increase the depth of field. The technique slightly reduces the light efficiency. Our detailed analysis has been based on the scalar diffraction theory. The conclusions of it could be heuristically understood in terms of simple ray-tracing arguments. However, such arguments would not permit to obtain precise values neither for the evolution of the lateral resolution, for the range of axial positions of the 3D object in which the lateral resolution is imposed by the detector pixel size. Moreover, the ray-tracing model would not allow analyzing the case of other more elaborate pupil functions as, for example, the annular pupils or the gaussian ones.

ACKNOWLEDGEMENTS

This work has been funded in part by the Plan Nacional I+D+I (grant DPI2003-4698), Ministerio de Ciencia y Tecnología, Spain. We also acknowledge the financial support from the Generalitat Valenciana, Spain (grant grupos03/227).

REFERENCES

1. J.-S. Jang and B. Javidi, "Three-dimensional integral imaging of micro-objects," Opt. Lett. **29**, 1230-1232 (2004).
2. H. Liao, M. Iwahara, N. Hata and T. Dohi, "High-quality integral videography using multiprojector," Opt. Express **12**, 1067-1076 (2004).
3. S. A. Benton, ed., Selected Papers on Three-Dimensional Displays (SPIE Optical Engineering Press, Bellingham, WA, 2001).
4. D. H. McMahon and H. J. Caulfield, "A technique for producing wide-angle holographic displays," Appl. Opt. **9**, 91-96 (1970).
5. P. Ambs, L. Bigue, R. Binet, J. Colineau, J.-C. Lehureau, and J.-P. Huignard, "Image reconstruction using electro-optic holography," *Proc. of the 16th Annual Meeting of the IEEE Lasers and Electro-Optics Society, LEOS 2003,* vol. 1 (IEEE, Piscataway, NJ, 2003) pp. 172-173
6. T. Okoshi, "Three-dimensional displays," Proc. IEEE **68**, 548-564 (1980).
7. M. G. Lippmann, “Epreuves reversibles donnant la sensation du relief,” J. Phys. (Paris) **7**, 821-825 (1908).
8. H. E. Ives, "Optical properties of a Lippmann lenticuled sheet," J. Opt. Soc. Am. **21**, 171-176 (1931).
9. C. B. Burckhardt, "Optimum parameters and resolution limitation of integral photography," J. Opt. Soc. Am. **58**, 71-76 (1968).
10. T. Okoshi, "Optimum design and depth resolution of lens-shet and projection type three-dimensional displays," Appl. Opt. **10**, 2284-2291 (1971).
11. N. Davies, M. McCormick and L. Yang, "Three-dimensional imaging systems: a new development," Appl. Opt. **27**, 4520-4528 (1988).
12. N. Davies, M. McCormick and M. Brewin, "Design and analysis of an image transfer system usig microlens array," Opt. Eng. **33**, 3624-3633 (1994).
13. F. Okano, H. Hoshino, J. Arai and I. Yayuma, "Real time pickup method for a three-dimensional image based on integral photography," Appl. Opt. **36**, 1598-1603 (1997).
14. J. Arai, F. Okano, H. Hoshino and I. Yuyama, "Gradient-index lens-array method based on real-time integral photography for three-dimensional images," Appl. Opt. **37**, 2034-2045 (1998).
15. L. Erdmann and K. J. Gabriel, "High resolution digital photography by use of a scanning microlens array," Appl. Opt. **40**, 5592-5599 (2001).
16. S. Kishk and B. Javidi, "Improved resolution 3D object sensing and recognition using time multiplexed computational integral imaging," Opt. Express **11**, 3528-3541 (2003).
17. A. Stern and B. Javidi, “Three-dimensional image sensing and reconstruction with time-division multiplexed computational integral imaging”, Appl. Opt. **42**, 7036-7042 (2003).
18. J.-S. Jang and B. Javidi, "Three-dimensional synthetic aperture integral imaging," Opt. Lett. **27**, 1144-1146 (2002).
19. J.-S. Jang and B. Javidi, "Improved viewing resolution of three-dimensional integral imaging by use of nonstationary micro-optics," Opt. Lett. **27**, 324-326 (2002).
20. J.-S. Jang and B. Javidi, "Large depth-of-focus time-multiplexed three-dimensional integral imaging by use of lenslets with nonuniform focal lengths and aperture sizes," Opt. Lett. **28**, 1924-1926 (2003).
21. M. Martínez-Corral, B. Javidi, R. Martínez-Cuenca, and G. Saavedra, “Integral imaging with improved depth of field by use of amplitude modulated microlens array”, Appl. Opt. (in press).
22. H. Choi, S.-W. Min, S. Jung, J.-H. Park and B. Lee, "Multiple-viewing-zone integral imaging using dynamic barrier array for three-dimensional displays," Opt. Express **11**, 927-932 (2003).

23. J. Arai, H. Hoshino, M. Okui and F. Okano, "Effects on the resolution characteristics of integral photography," J. Opt. Soc. Am. **20**, 996-1004 (2003).
24. H. Hoshino, F. Okano, H. Isono and I. Yuyama, "Analysis of resolution limitation of integral photography," J. Opt. Soc. Am. A **15**, 2059-2065 (1998).
25. J.-H. Park, S.-W. Min, S. Jung and B. Lee, "Analysis of viewing parameters for two display methods based on integral photography," Appl. Opt. **40**, 5217-5232 (2001).
26. M. Martínez-Corral, B. Javidi, R. Martínez-Cuenca and G. Saavedra, "Multifacet structure of observed reconstructed integral images," J. Opt. Soc. Am. A **22**, 597-603 (2005).
27. J.-S. Jang, F. Jin, and B. Javidi, "Three-dimensional integral imaging with large depth of focus by use of real and virtual image fields," Opt. Lett. **28**, 1421-1423 (2003).
28. B. Lee, S.-W. Min, S. Jung, and J.-H. Park, "Computer generated dynamic three-dimensional display using integral photography adopting Fesnel lensens," Proc. SPIE **4471**, 9-17 (2001).
29. J.-S. Jang and B. Javidi, "Large depth-of-focus time-multiplexed three-dimensional integral imaging by use of lenslets with nonuniform focal lengths and aperture sizes," Opt. Lett. **28**, 1924-1926 (2003).
30. M. Martínez-Corral, B. Javidi, R. Martínez-Cuenca and G. Saavedra, "Integral imaging with improved depth of field by use of amplitude-modulated microlens array," Appl. Opt. **45**, 5806-5813 (2004).
31. R. Martínez-Cuenca, G. Saavedra, M. Martínez-Corral and B. Javidi, "Enhanced depth of field integral imaging with sensor resolution constraints," Opt. Express **12**, 5237-5242 (2004).
32. A. E. Siegman, *Lasers* (Univ. Science, Saulito, CA 1986).
33. A. Stokseth, "Properties of a Defocused Optical System," J. Opt. Soc. Am. **59**, 1314-1321 (1969).
34. C. J. Zapata-Rodríguez, P. Andrés, M. Martínez-Corral, and L. Muñoz-Escrivá, "Gaussian imaging transformation for the paraxial Debye formulation of the focal region in a low-Fresnel-number optical system," J. Opt. Soc. Am. A **17**, 1185-1191 (2000).
35. M. Martínez-Corral, C. Ibáñez-López, G. Saavedra, and M. T. Caballero, "Axial gain resolution in optical sectioning fluorescence microscopy by shaded-ring filters," Opt. Express **11**, 1740-1745 (2003).
36. C. Ibáñez-López, G. Saavedra, G. Boyer and M. Martínez-Corral, "Quasi-isotropic 3-D resolution in two-photon scanning microscopy," Opt. Express **12**, 6168-6174 (2005).